# Power Loss Tracking for the PEM Electrolyser using Multiphysics Dynamical Bond Graph model

Mahdi Boukerdja[1], Sumit Sood[1,*], Belkacem Ould-Bouamama[1], Anne-Lise Gehin[1], Abd Essalam Badoud[b]

[a] *Université de Lille, CRIStAL - Centre de Recherche en Informatique Signal et Automatique de Lille, UMR 9189 CNRS*
*59650 villeneuve Dascq, France, mahdi.boukerdja@univ-lille.fr, sumit.sood@univ-lille.fr, belkacem.ouldbouamama@polytech-lille.fr, anne-lise.gehin@univ-lille.fr*
[b] *Setif Automatic Laboratory, Department of Electrical Engineering, Setif 1 University, Setif, Algeria, badoudabde@univ-setif.dz*

**Abstract**

Green hydrogen generation using intermittent renewable sources through electrolysis faces challenges related to efficiency and reliability, largely due to material limitations and the fluctuating nature of energy inputs. These fluctuations disrupt continuous hydrogen production and increase the degradation rate of various components of the electrolyser, leading to power losses and diminished performance. To address this, a bond graph model-based power loss tracking approach is proposed to study the impact of degradation on Proton Exchange Membrane (PEM) electrolyser performance. This approach enables real-time tracking of power losses at different subcomponent and physical phenomenon levels by accurately representing the system's reaction kinetics and complex, nonlinear, multi-physical dynamics. Implemented in the 20-Sim software, the model benefits from automatic generation of governing analytical equations, enhancing usability and insight. A sensitivity study of the model has also been performed to analyse the responsiveness of the power loss trackers to the change in parameters. The model can serve as a valuable tool during the design phase, allowing engineers to analyse and estimate power losses under various operating conditions. A simulation-based validation was conducted within a green hydrogen production multisource platform, confirming the model's capabilities. Due to its causal and structural properties, the developed approach has the potential to support diagnostics and prognostics of a PEM electrolyser.

*Keywords:* Efficiency Tracking; Coupled Bond Graph; PEM Electrolyser; Diagosis; Multi-physical Modelling; Green Hydrogen; Power Losses; Reliability

*Corresponding author

**Nomenclature**

| | | | |
|---|---|---|---|
| $\Delta G_R$ | Gibb's free energy required for dissociation of water, J.mol$^{-1}$ | $M_i$ | Molar mass for the $i^{th}$ species, kg mol$^{-1}$ |
| $\dot{\xi}$ | Reaction flow rate, mol.s$^{-1}$ | $n_{eo}$ | Electro-osmosis drag coefficient |
| $\dot{H}$ | Rate of change of enthalpy, J.s$^{-1}$ | $P$ | Pressure, Pa |
| $\dot{m}_i$ | Mass flow rate for the $i^{th}$ species , kg.s$^{-1}$ | $p_i^j$ | Partial pressure of the $i^{th}$ species on $j^{th}$ electrode side, Pa |
| $\dot{n}_i$ | Molar flow for the $i^{th}$ species, mol.s$^{-1}$ | $R_j^{hy}$ | Internal fluidic resistance of the cell for the $j^{th}$ electrode side, Pa.s.kg$^{-1}$ |
| $\dot{Q}$ | Heat flow rate, J.s$^{-1}$ | $R_c$ | Multiport resistive element for coupling between fluidic and thermal flows |
| $\nu_i$ | Stoichiometric Coefficient for the $i^{th}$ species | $R_{cell}^{th}$ | Thermal resistance of the PEM electrolysis cell, J.$K^{-1}$ |
| $a_{H_2O}$ | Chemical activity of water | $R_{diff,i}$ | Diffusion resistance of the $i^{th}$ species, Pa.s.kg$^{-1}$ |
| $C_{cell}^{th}$ | Thermal capacitance of the PEM electrolysis cell, J.$K^{-1}$ | $R_{ohmic}$ | Ohmic resistance of the cell, $\Omega$ |
| $C_{dl}$ | Dual layer capacitance, F | $RS$ | Multiport resistive element for irreversible transformation of electical energy to thermal energy |
| $C_j$ | Fluidic storage capacity of the $j^{th}$ electrode side, kg$^2$.J$^{-1}$ | $T$ | Temperature, K |
| $E_{act,j}$ | Activation overpotential for the $j^{th}$ electrode, V | $w_{j,i}$ | Mass fraction of the $i^{th}$ species for the $j^{th}$ electrode side |
| $E_{cell}$ | Overall cell voltage, V | $\beta$ | Diffusion Coefficint, m$^2$.s$^{-1}$ |
| $E_{con}$ | Concentration overpotential, V | $\mu_i$ | Chemical potential of the $i^{th}$ species, J.kg$^{-1}$ |
| $E_{ohmic}$ | Ohmic overpotential, V | A$_i$ | Chemical affinity of the $i^{th}$ species, J.mol$^{-1}$ |
| $E_{rev}$ | Reversible cell voltage, V | F | Faraday's constant, C.mol$^{-1}$ |
| $E_{rev}^0$ | Standard reversible cell voltage at standard operating consitions, V | | |
| $I_{0,k}$ | Standard current exchange density for $k^{th}$ electrode, A.m$^{-2}$ | | |
| $I_{cell}$ | Total cell current, A | | |
| $I_{lim}$ | Limiting current due to mass transport phenomena, A | | |

## 1. Introduction

Proton Exchange Membrane (PEM) electrolysers are playing a crucial role in the transition toward a cleaner and more sustainable energy system. Its advantages over alkaline electrolysis, such as rapid response to the change in operating conditions, ability to operate at higher pressure, higher purity of the hydrogen, and compact size, make it the best choice for surplus renewable energy storage, such as solar energy and wind energy, as an alternative to the batteries in the form of green hydrogen during off-peak hours [1]. This coupling of the PEM electrolysers with intermittent energy sources interests the researchers for numerous reasons. PEM electrolysers are highly responsive to fluctuations in electricity supply, and their fast startup times and ability to quickly ramp up or down in response to changes in input power make them ideal for use with intermittent renewable energy sources to have efficient operation. PEM electrolysers help unlock the full potential of clean energy and contribute to a decarbonised future. PEM electrolysis paired with renewable energy sources helps accelerate the transition by providing a viable way to store and use renewable energy at scale. However, despite these advantages of the PEM electrolyser, ensuring the reliability of the system and efficient operation of the electrolyser when operated with intermittent renewable energy sources is still a challenge.

The intermittency of renewable energy sources results in poor performance and lower efficiency of the electrolyser due to water and gas transport issues emerging from variations in the flow of hydrogen and the accumulation of gases at the reaction site. The intermittency of the energy sources can also accelerate the degradation of the electrolyser by inducing mechanical and thermal stresses in the electrolyser cell/ stack [2]. This further reduces the performance and useful life of the electrolyser. Also, the complexity in the operation of the electrolysis due to the involvement of the different physical phenomena that are also tangled with each other makes the prediction of the performance of the electrolyser very difficult. The performance of the electrolyser design is traditionally analysed by testing the electrolyser under a controlled environment at different operating conditions [3]. However, the operating conditions during the actual commissioning of the electrolyser system may differ from those used for its performance assessment, and this might lead to an underperforming system. Also, it is important to mention that this method of performance analysis is quite expensive and time-consuming. The electrolyser cell/ stack is a complex component, and slight variations during its manufacturing can also lead to significant performance differences. For example, the tightening of the bolts that hold the electrolysis stack together has a significant impact on the mechanical stresses on the membrane, which can affect the overall performance of the stack by accelerating the degradation. Thus, this method of performance analysis can only give a general idea of the electrolyser. The solution to this problem is to use the simulation environment to analyse the performance of the electrolyser, which can reduce the overall design and testing cost significantly.

Efficiency tracking plays a major role in reaping the maximum benefits from coupling PEM electrolysers with intermittent energy sources. It helps to im-

prove the durability of the PEM stack by estimating power losses caused by degradation, which are not captured by measurement instruments. This information not only acts as the performance indicator for the system but also can be used to analyse the evolution of the power losses over time, which directly reflects the degradation speed of PEM stack components such as the membrane and electrodes. This aids in making better design decisions for choosing the best materials used to manufacture PEM electrolyser stacks. Power loss estimates can also serve as indicators for fault detection and isolation within the PEM stack, especially if these losses are due to degradation. Estimating power losses allows for operating the PEM stack in a degradation-tolerant manner by adopting a suitable operating point by controlling the actuators, including pumps and converters that supply water and electricity to the PEM stack, which can be continuously adapted to compensate for power loss due to degradation. The Bond Graph models are well-suited for efficiency tracking or power loss estimation, as the models are based on the power/ energy exchange between the elements representing the physical phenomena and components. Different subcomponents can also be modelled as submodels in a modular fashion, also known as capsules among Bond Graph users, thus portraying the power interaction between different subcomponents [4]. This makes the monitoring of the power exchange within the electrolyser among various subcomponents feasible, ultimately allowing the tracking of the power losses at different phenomena or subcomponent levels, provided that the Bond Graph model is accurate enough to truly represent the actual PEM electrolyser system. This, of course, requires the researchers to model all the key phenomena and to identify the model parameters with reasonable accuracy, which is almost practically impossible. This problem, however, can be tackled by combining the Bond Graph models with Linear Fractional Transformation (LFT) to include the effect of measurement and parameter uncertainties.

Over the years, researchers have proposed various Bond Graph models for PEM electrolysers for performance simulation, control diagnosis, and prognosis. The model developed by Olivier et al. [5], for an industrial PEM electrolyser, has taken into account the stack as well as the Balance of Plant (BoP) for the simulation of the dynamic behaviour of PEM electrolyser for the estimation of the power consumption and prediction of stack temperature. However, due to the high complexity of the model, it cannot be easily scaled or adapted for other types of electrolysers. Also, the model was not exploited for diagnosis and prognosis, but only for analysis. Another Bond Graph model was developed by Sood et al. [6] for the performance simulation of the PEM electrolyser running on renewable energy sources and was implemented on the laboratory-sized single-cell PEM electrolyser. The developed model was also utilised for diagnosis using LFT Bond Graph [7, 8]. Another work showcases how the Bond Graph model of a single cell PEM electrolyser can be exploited for estimating the remaining useful life of a PEM electrolysis cell [9]. In another work, researchers have proposed the Bond Graph model for the hybrid power system that includes the PEM water electrolysis to generate hydrogen from solar energy and proposed the control strategy based on power flow management. Correa et al. [10] pro-

posed a lumped parameter Bond Graph model for a PEM electrolysis stack of 5.6 kW to analyse the effect of the temperature on the activation overpotential of the cathode side and the performance of high-pressure PEM electrolysers.

Other modelling techniques have been utilised to model PEM electrolysers and are mostly utilised to develop a digital twin for a PEM electrolyser stack. In [11], a simple analytical model is used to create a numerical replica of the PEM stack that interacts with system measurements. The objective of this model is to monitor the system and to detect and isolate faults. In [12], the PEM stack is modelled using a physics-informed neural network technique, which is applied to monitor the stack's performance and to estimate the inlet temperature. In [13], a digital twin is developed based on an analytical model that incorporates physical knowledge of electrochemical and thermodynamic phenomena. This digital twin is used to estimate the temperature of the stack cells, supporting effective thermal management of the electrolyser. In [14], the digital twin integrates a backpropagation neural network model for electrochemical performance analysis, along with a lumped thermal capacitance model for thermal performance assessment. This approach enables real-time monitoring and selection of optimal control variables for improved operation. However, these digital twins have primarily been applied for monitoring and control of the PEM electrolyser stack and have not yet addressed the estimation of degradation impact manifested as power losses.

These research works have proven the capability of the modelling approach in handling the complexity of the PEM electrolyser for various applications. However, none of them have exploited these models for online efficiency/ power loss tracking. Therefore, in this article, an innovative approach for exploiting the multiphysics dynamical model of PEM electrolysis cell based on coupled Bond Graph theory for real-time efficiency/ power loss tracking has been proposed. The proposed model can capture the key dynamics and the reaction kinetics of the PEM electrolysis cell, such as electrothermal, electrochemical, and thermofluidic phenomena and incorporate the proposed power loss trackers, which are the part of the proposed model, for estimating the power loss initiated by the degradations and faults. It is important to mention that in most of the previous works cited, the developed models have finally been implemented in MATLAB Simulink by converting the Bond Graph model into a Block Diagram Representation. This, however, causes the loss of one of the important characteristics of the Bond Graph models, i.e., to automatically generate the system equations directly from the Bond Graph model. This means that the models presented in the cited work can not be easily modified or adapted to different configurations of the PEM electrolyser. The Bond Graph model proposed in this work has been developed in the form of capsules using 20-Sim software, which has been designed and maintained by Controllab of the University of Twente of the Netherlands [15]. This software allows the user to exploit the full potential of the Bond Graph tool, as the system equations and fault indicators are automatically generated, which makes the developed model easily adaptable for different configurations of the PEM electrolyser. Another innovative interest of the proposed approach is that the power loss indicators can also be used

for degradation estimation, and complex degradation models can be avoided for remaining useful life estimation, compared to those models conventionally developed in the literature consulted. The effectiveness of the proposed approach has been demonstrated through various simulations validated in a real electrolyser.

The article is further segregated into four parts. Section 2 provides a brief introduction to the coupled Bond Graph theory for online efficiency/ power loss tracking of multiphysics systems. Section 3 is dedicated to the discussion of the Bond Graph model of the PEM electrolysis cell. Section 4 presents the simulations and the discussion of the effectiveness of the proposed approach. Section 5 portrays the conclusion and future perspectives of the proposed work.

## 2. Coupled Bond Graph approach for efficiency tracking

A coupled Bond Graph is well suited for the modelling of multiphysics phenomena using a handful of elements representing the elementary physical property or energy interaction within the system. The coupled Bond Graph approach has been presented briefly in the following subsection and can be found in detail in different books and articles [16, 17, 18].

### *2.1. Coupled Bond Graphs*

Bond Graphs are the graphical representation of the energy flow in a system in the form of various elements (fundamental building blocks) that represent the basic physical property of the system, such as energy storage, energy dissipation and energy transformation and the interaction of these elements with each other to constitute the behaviour of the system. Bond graphs are versatile tools for modelling and analysing systems across different physical domains by representing energy flow using effort and flow variables. They unify the representation of different physical domains by defining domain-specific effort and flow variables while maintaining consistency in how the energy is exchanged. The generalised Bond Graph elements can be used for all physical domains. These elements include $C$: compliance element (potential energy storage), $I$: inertial element (kinetic energy storage), $Sf$: source of flow, $Se$: source of effort, $R$: resistive element (energy dissipation), energy transformation elements ($TF$: transformer and $GY$: gyrator) to transfer or transform energy between physical domains, virtual detectors ($Df$: flow detector and $De$ effort detector) to detect flow or effort in the Bond Graph. The sources of effort and flow can be constant or can be modulated and are represented using $MSe$ and $MSf$, respectively. These elements and their significance in different physical domains have been summarised in the table 1 [19, 20, 21]. These elements are connected through multi-port elements called junctions ($j$: 0- flow sum junction, also known as equal effort junction and 1- effort sum junction, also known as equal flow junction) that represent the law of conservation of energy.

Table 1. Bond Graph elements for various physical domains

| Domain | Energy Storage (C, I) | Dissipation (R) | Power Sources (Se, Sf) | Energy Conversion (TF, GY) |
|---|---|---|---|---|
| **Electrical** | **Capacitance (C):** $q = C \cdot V$ (Charge, Voltage) **Inductance (I):** $\phi = L \cdot I$ (Flux, Current) | **Resistance (R):** $V = R \cdot I$ | **Se:** Voltage source ($V$) **Sf:** Current source ($I$) | **TF:** Transformer (fixed effort-flow ratio) **GY:** Gyrator (cross-domain coupling) |
| **Thermal** | **Thermal Capacitance (C):** $Q = C_T \cdot T$ (Heat content, Temperature) | **Thermal Resistance (R):** $\dot{Q} = \frac{\Delta T}{R_T}$ | **Se:** Fixed temperature ($T$) **Sf:** Fixed heat flow ($\dot{Q}$) | **TF:** Heat exchanger **GY:** Thermal-mechanical coupling (e.g., Peltier effect) |
| **Chemical** | **Chemical Capacitance (C):** $N = C_c \cdot \mu$ ( Moles, Chemical potential) | **Chemical Resistance (R):** Represents the quantity of matter transported by diffusion of species, and also determines the speed of reaction. zero (an explosion) until infinite (no | **Se:** Fixed chemical potential ($\mu$) **Sf:** Fixed molar flow ($\dot{N}$) | **TF:** Transformation from reactants to product with modulus equal to Stoichiometric coefficients. **GY:** Electrochemical coupling (e.g., batteries) |
| **Fluidic** | **Fluid Capacitance ($C_f$):** $V = C_f \cdot P$ (Volume, Pressure,) **Fluid Inertance (I):** $\Phi = L_f \cdot \dot{m}$ (Mass flow rate, Momentum) | **Fluid Resistance (R):** $\Delta P = R_f \cdot \dot{m}$ (e.g., pipe friction) | **Se:** Fixed pressure ($P$) **Sf:** Fixed mass flow rate ($\dot{m}$) | **TF:** Hydraulic cylinder **GY:** Fluid-mechanical coupling (e.g., turbines) |

The elements and junctions are connected through half arrows known as power bonds and represent the power exchange as shown in Figure 1(a). The half arrow represents the direction of the power flow. Each power bond has two associated power variables called effort and flow represented by $e$ and $f$, respectively, as shown in the figure 1(a) and the product of which represents the instantenous power flow through that bond and depending on the values of effort and flow (being negative or positive) determines the direction of actual power flow. It is worth mentioning that the product of effort and flow has no physical meaning and does not represent power for some physical domains. For example, the product of chemical affinity (effort) and reaction flow rate(flow) for the chemical domain, the product of pressure (effort) and mass flow rate(flow) for the fluidic domain, etc., does not represent physical power. Table 2 shows different domains' effort and flow variables.

In Figure 1(a), the red vertical stroke on the power bond represents causality, which is a fundamental concept in bond graph modelling. Causality defines the direction of information flow between elements and determines how the two power variables are related. In any power interaction, one of these variables is

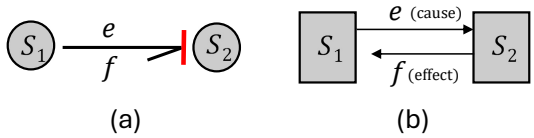


Figure 1. Power bond in Bond Graph modelling:(a) Representation and (b) Interpretation.

treated as the independent variable (the "cause"), while the other is computed as the dependent variable (the "effect") as shown in Figure 1(b). The red stroke is placed at the end of the bond where the effort is supplied or known, and it indicates that effort flows into that element from the connected component. This means the element with the stroke is receiving effort information and will respond by computing or generating the corresponding flow variable.

Causality plays a crucial role in the formulation and simulation of dynamic models using bond graphs. By assigning causal strokes consistently across the entire graph, it becomes possible to determine the order in which equations should be solved and how subsystems interact. For example, in storage elements such as inertias (I-elements) and capacitors (C-elements), the correct assignment of causality is necessary to properly capture the energy storage and dynamic behaviour of the system. Improper causality assignments can lead to modelling errors or algebraic loops in simulation. Modern software like 20-Sim can assign the causality automatically. For the storage elements, two types of causality are possible, namely integral causality and derivative causality, and both types of causality serve different purposes for the implementation of the Bond Graph model. Figure 2 shows the inertial storage element in (a) integral causality and (b) derivative causality.

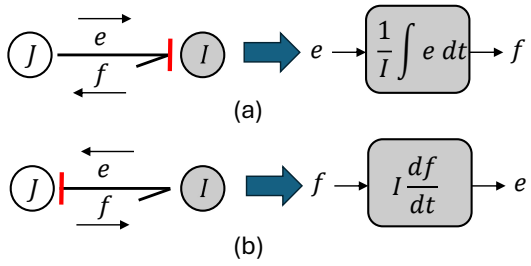


Figure 2. Bond Graph representation of inertial element in (a) integral causality and (b) differential causality.

In the integral causality configuration, as shown in Figure 2(a), the causality stroke is towards the $I$ element. Thus, the I element receives the effort information from the junction and returns the flow information to the junction. Here, the effort and flow are the cause and the effect, respectively, and the flow is the integral of the effort over time. Integral causality is preferred for the energy storage element ($I$ and $C$ elements) when the initial values of the states can be

defined. This is helpful when the Bond Graph model is used for the performance simulation based on the specified initial conditions. Figure 2(b) represents the derivative causality as the effect (effort in the case of $I$ element) is the time derivative of the cause (flow in the case of $I$ element). Derivative causality for storage elements is particularly helpful in the case of Bond Graph-based diagnosis.

Table 2. Bond Graph power variables for different physical domains[4, 5, 22].

| **Physical domain** | **Effort variable (units)** | **Flow variable (units)** |
|---|---|---|
| Electrical domain | Voltage (V) | Current (A) |
| Thermal domain | Temperature (K) | Entropy flow rate($J.K^{-1}.s^{-1}$)<br>Heat flow rate ($J.s^{-1}$) |
| Chemical domain | Chemical potential ($J.mol^{-1}$)<br>Chemical affinity ($J.mol^{-1}$) | Molar flow rate ($mol.s^{-1}$)<br>Reaction flow rate ($mol.s^{-1}$) |
| Fluidic domain | Pressure (Pa) | Volume flow rate ($m^3.s^{-1}$)<br>Mass flow rate ($kg.s^{-1}$) |

The conventional bond graph approach primarily focuses on representing power exchange between individual components and subsystems through power bonds that signify instantaneous power flow (product of effort and flow variables). While effective for simpler systems that do not have multiple domains interactions, it can become cumbersome for complex multiphysics systems where strong interdependencies exist between different energy domains (e.g., electrical, thermal, fluidic etc.). Coupled Bond Graph extends the capabilities of the regular Bond Graph approach to address the complexity of multiple physical domains' interaction and entanglement using the modified elements such as those been presented in figure 3, making it a robust tool for analysing complex systems, such as in the case of PEM electrolysers. For example, the modified form of the resistive element, represented by $RS$ as shown in 3(a), is used to model the irreversible transformation of electric energy into heat, such as in the case of electrical resistance taking into account the production of entropy [23]. The coupling between thermal and fluidic domains is represented using a multiport resistance element ($R_C$) as shown in Figure 3(b) [5, 6]. Some authors have also represented it with the coupling element for thermo-fluidic (CETF) [24] that comprises a modulated source of flow representing the enthalpy flow rate as shown in figure 3(c). The compliance element of a thermofluidic system is also coupled as the thermal capacity of such a system is directly linked to the amount of fluid in the system, thus entangled with the fluidic capacity of the system and can be represented using a lumped parameter [5, 6].

Bond graph modelling follows a systematic, structured approach with four different levels of abstraction, progressively refining the system representation for analysis and simulation [17]. The first level is the physical system level at which the physical system is identified, consisting of various energy domains such

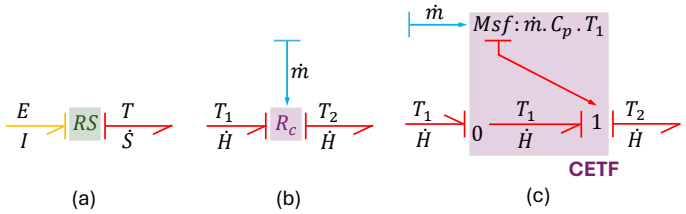


Figure 3. Coupled Bond Graph elements for coupling of phenomenon

as mechanical, electrical, fluidic, thermal, chemical or mixed-domain systems. The components of the system and their energy interactions are clearly defined. This stage focuses on understanding how energy flows through the system and identifying key elements that store, dissipate, or transfer energy. The second level is the graphical model level, at which the physical system is represented using a bond graph, a graphical representation of energy flow based on power variables (effort and flow) using the Bond Graph elements to model energy storage, dissipation, and conversion. Junctions define energy connections, ensuring the proper interconnection of elements. Causality is assigned to each bond, specifying whether a variable (effort or flow) is an input or an output, which is essential for deriving mathematical equations. The third level is the mathematical model level; the bond graph is systematically converted into a system of equations that describe the dynamics of the system. Using constitutive relations, the system is formulated in terms of differential and algebraic equations. The mathematical model provides a structured and modular representation that facilitates further analysis, including stability, controllability, and system response evaluation. Finally, at the simulation/computation level, the mathematical model is implemented in computational tools such as MATLAB/Simulink, 20-sim, or Modelica for numerical simulation. These tools solve the differential equations using numerical integration methods (e.g., Runge-Kutta) to predict system behaviour under various conditions. By following this hierarchical approach, bond graph modelling ensures a seamless transition from a physical system to an executable simulation, making it a powerful tool for complex multi-domain system analysis and design. For the presented work, 20-sim has been chosen as the preferred platform for the development and implementation of the bond graph model of PEM electrolyser. It is a powerful tool for bond graph modelling due to its native support for multi-domain system simulation, intuitive graphical interface, and automatic equation generation directly from the graphical model [25]. It seamlessly integrates mechanical, electrical, hydraulic, and thermal systems, making it ideal for complex, multi-physics modelling. 20-sim also supports the encapsulation of the Bond Graph model of different components and phenomena in the form of a .emx file (Encapsulated Model Exchange) so that the modular approach can be used to build complex models while allowing flexibility. The software also supports real-time simulation, optimisation, and hardware-in-the-loop (HIL) applications, enabling efficient control system

design.

### *2.2. Bond Graph-based efficiency/ power loss tracking*

To calculate efficiency, the input and output of the system or subsystem must be known with certainty. However, these values may not always be directly measurable at the subcomponent level, either due to the absence of the required sensors or the quantity being unmeasurable using sensors. In such cases, a mathematical model can be employed to estimate power losses, enabling efficiency calculations for various subcomponents or sub-elements. Virtual sensors can assist in estimating the power variables needed for power loss calculations. Figure 4 shows the proposed methodology to estimate the power loss using a Bond Graph approach. The image shows the two power loss estimators that have been proposed based on the sensor information type and are modelled as capsules in 20-Sim. This provides the modularity and reusability, thus allowing the user to exploit these power loss trackers as part of the Bond Graph library as and when required. These estimators are labelled as Power Loss Tracker Effort Sensor type (PLTES), shown in Figure 4(a) and Power Loss Tracker Flow Sensor type (PLTFS), shown in Figure 4(b), for the presented work.

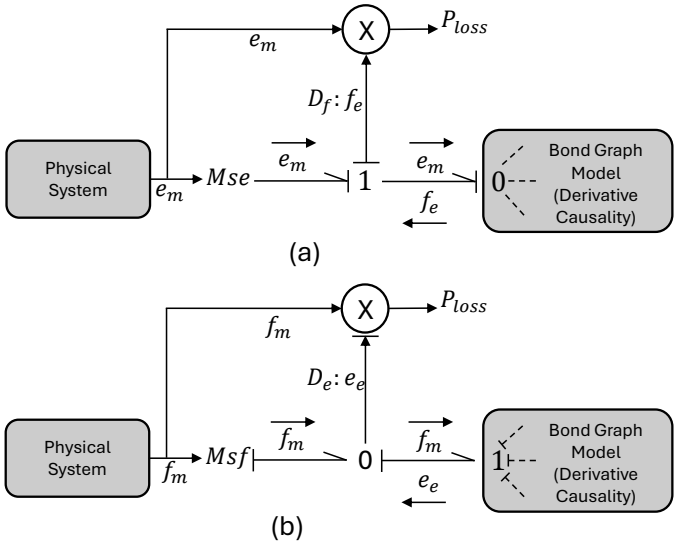


Figure 4. Power loss estimation capsules for Bond Graph Model, (a) PLTES and (b) PLTFS

For power loss estimation, the bond graph in derivative causality is preferred as it eliminates the requirement of the initial conditions. The measurements from the system are introduced as inputs to the derivative bond graph by dualising the system sensors [17]. For PLTES, the input is introduced as the modulated source of effort, as shown in the figure 4(a). For example, temperature, pressure, etc. measurements ($e_m$) are introduced as modulated sources of effort through 1 junction as shown in Figure 4(a). The power bond joining

the 1 junction to the derivative bond graph model is called a strong bond, as it sets the value of effort in all the power bonds connected to the 0 junction in the derivative bond graph model. As the 0 junction corresponds to the conservation law, the sum of the power entering and exiting the 0 junction must be equal to zero. In other terms, the sum of all the flows at this zero junction must be zero, i.e.,

$$\sum_{i=1}^{n} P_i = 0 \text{ or } \sum_{i=1}^{n} f_i = 0 \tag{1}$$

where $i$ represents the $i^{th}$ power bond and corresponding flow value, and $n$ represents the total number of power bonds connected to the 0 junction. Depending on the direction of the power, its numerical value is considered positive for the power entering the junction and negative for the power leaving the junction. This equation is valid for normal operating conditions, while the parametric and measurement errors are assumed to be negligible or non-existent. In the case of the non-negligible uncertainties, the LFT bond graph must be used to calculate the thresholds that bound the non-zero value of the equation 1 [8]. The numerical value of the equation 1 is termed as a residual and is often used for diagnosis. When a fault occurs in the system to which the particular residual is sensitive, the value of the residual becomes non-zero or crosses the thresholds in the case of the LFT bond graph. This change in the residual value can also be used to track the power loss due to the fault. The change in the residual value is equal to the flow in the power bond connecting the effort measurement to the derivative bond graph, represented by $f_e$ in Figure 4(a). This flow can be measured using the flow detector ($D_f$) at the 1 junction, as shown in the figure, and the product of this estimated flow with the measurement from the sensor gives the value of the instantaneous power loss corresponding to the fault that occurred. Similarly, power loss can be estimated using PLTFS using the measurements ($f_m$) of the flow variables such as current, mass flow rate, etc., as shown in Figure 4(b).

Figure 5 shows the example of the power loss tracking using the proposed methodology for a water tank of fluidic capacity $C_f$ being filled with a pump at $Q_{in}$ flow rate.

A sensor measures the height $h$ of the water level in the tank, which can be considered as an effort type sensor as the measurements from the sensor can be used to calculate the water pressure inside the tank, i.e. $\rho.g.h$. The exit valve can be modelled as a fluidic resistance $R_f$ whose value is inf when the valve is closed and 0 when the valve is fully open. The fault in the position of the valve can lead to the loss of water, which corresponds to the loss of fluidic power. This power loss can be tracked using PLTES as shown in Figure 5. The height sensor is dualised and used as the modulated source of effort to provide tank pressure as input to the diagnostic bond graph of the system. From the diagnostic bond graph model, the flow (leakage due to fault in valve) is estimated from the conservation law at the 0 junction, which is given by the equation 2

$$f_e = C_f \frac{dp}{dt} + \frac{e_m - P_{out}}{R_f} - Q_{in} \tag{2}$$

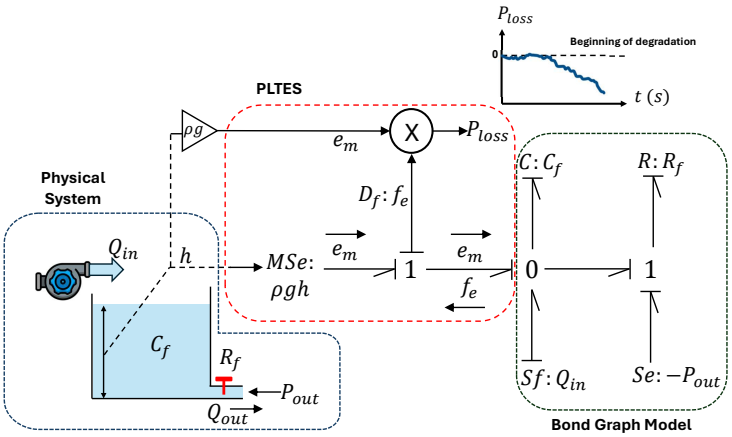


Figure 5. Power loss estimation using proposed methodology

The product of the estimated flow and the effort measured from the sensor gives the power loss. This power loss tracking also corresponds to the loss in the efficiency of the system and can be used to monitor the performance and health of the system. This also gives scope to utilise the power loss tracking for estimating the remaining useful life of the system if the evolution of the power loss can be predicted, it can be exploited for the estimation of remaining useful life. In the absence of the actual measurements, the performance model of the system can be used with virtual sensors to provide the measurements. This approach has been implemented in this article. As it is difficult and dangerous to introduce faults in the actual system, the performance model provides the perfect opportunity to test the proposed methodology, as various faults can be introduced in the performance model at any instant and with different evolution conditions.

## 3. Coupled Bond Graph Model of PEM electrolyser cell

PEM electrolysis cell is a complex multiphysics system due to the entanglement of different physical domains as depicted in Figure 6.

Due to this complexity, the coupled bond graph approach is well-suited to develop the model of the PEM electrolysis cell/ stack. The model consists of various submodels/capsules representing different physical phenomena coupled together, such as electrothermal, electrochemical and thermofluidic phenomena that interact with each other to provide the holistic model. The interactions between these submodels are shown in Figure 7, also showing the inputs and outputs for different submodels.

The expanded bond graph model (in derivative causality) for the PEM electrolysis cell is shown in Figure 8. Different phenomena-based submodels have been highlighted, and the interaction between these submodels can be seen near

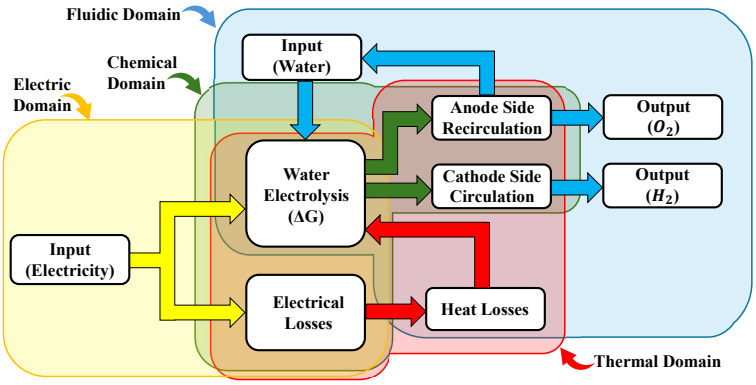


Figure 6. Coupling of various phenomena in PEM water electrolysis.

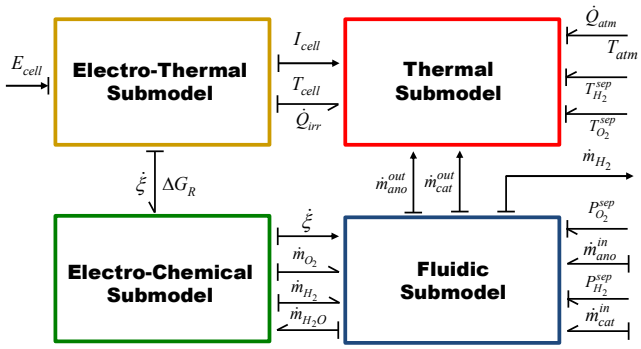


Figure 7. Phenomena-based submodels of PEM electrolysis cell and their interactions.

the boundaries of these submodels. Different coloured bonds are used in the figure to represent power bonds of different energy domains: yellow for electrical, red for thermal, blue for fluidic, and green for chemical. The presented model is the improved version of the Bond Graph model developed and presented by the authors in previous work [6, 8]. The model has been modified for the implementation in 20-sim, and these modifications have been highlighted in the subsequent paragraphs.

The electro-thermal submodel, in Figure 8, is responsible for the estimation of the electrical power losses due to ohmic resistance of the Membrane Electrode Assembly (MEA), activation overpotentials and concentration polarisation due to the concentration gradient of different species. These power losses have been modelled as the multiport resistance elements, and the electrical losses due to these resistances contribute to the irreversible heat flow that increases the temperature of the cell. The dual-layer capacitance of the cell is modelled as a compliance element ($C_{dl}$), which is responsible for the accumulation of the charge during the transient behaviour of the cell. The dual-layer capacitance is

given as [26]

$$C_{dl} = \varepsilon \frac{A}{d_{dl}} \tag{3}$$

where $\varepsilon$ is electrolyte permittivity, $A$ is electrode's surface area and $d_{dl}$ is

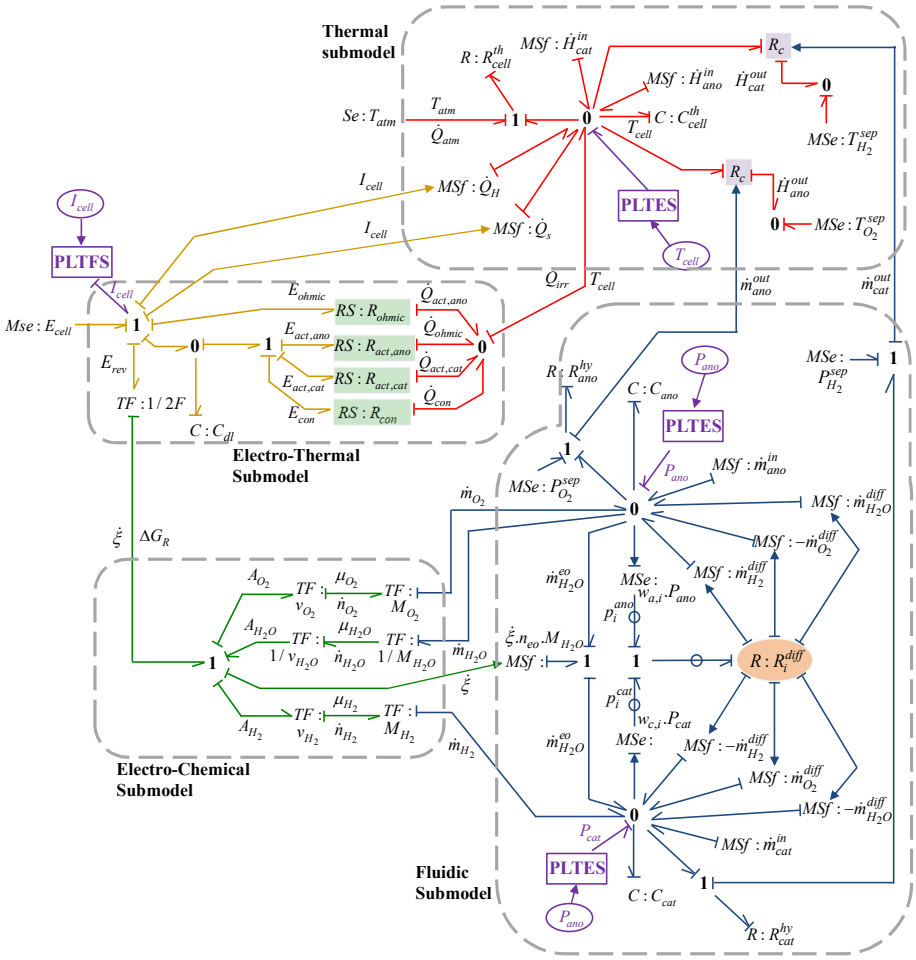


Figure 8. Bond graph model of PEM electrolysis cell in derivative causality for power loss tracking.

thickness of the dual layer. The cell voltage can be calculated from the junction equation as

$$E_{cell} = E_{ohmic} + E_{act,ano} + E_{act,cat} + E_{rev} + E_{con} \tag{4}$$

The equations representing the non linear resistances in the eletro-thermal sub-model have been discussed in details in [6, 8]. Substituting the values of voltages

in right hand side based on the equations from [6, 8], the cell voltage can be written as

$$E_{cell} = R_{ohmic}.I_{cell} + \frac{R.T_{cell}}{F}\sinh^{-1}\left(\frac{I_{cell}}{2.I_{0,a}}\right) + \frac{R.T_{cell}}{F}\sinh^{-1}\left(\frac{I_{cell}}{2.I_{0,c}}\right) + E^0_{rev} + \frac{R.T_{cell}}{2.F}ln\left(\frac{{p_{H_2}.p_{O_2}}^{1/2}}{a_{H_2O}}\right) + \frac{R.T_{cell}}{2.\beta.F}\ln\left(1+\frac{I_{cell}}{I_lim}\right) \tag{5}$$

The electrochemical sub-model is responsible for calculating the production of hydrogen, oxygen and water consumption. It also calculates the energy (Gibbs free energy) required for the dissolution of water into the gases, which enables the calculation of reversible voltage. The rate of production of the hydrogen is calculated using the equation [6]

$$\dot{m}_{H_2} = \nu_{H_2}.M_{H_2}.\dot{\xi} = \nu_{H_2}.M_{H_2}.\frac{I_{cell}}{2.F} \tag{6}$$

The fluidic submodel is based on the conservation of mass flow to estimate the pressure on the anode and the cathode side because of the flow of water and produced gases. The model takes into account the effect of electro-osmosis drag and diffusion of gases from one side to another, and the water from the anode to the cathode side. These flows have been modelled as the modulated sources of flow to simplify the model to be implemented in 20-sim. The diffusion is modelled as a multiport resistance element. In the thermal sub-model, the lumped parameter approach has been followed to model the thermal resistance and thermal capacity of the PEM electrolysis cell. These parameters are responsible for the evolution of the temperature of the electrolysis cell over time. Using a lumped thermal capacity for a PEM electrolysis cell simplifies the thermal modelling process by assuming that the entire cell maintains a uniform temperature throughout. The choice of the lumped parametric approach can also be justified through the fact that the similar assumption is also made in experimental study of the PEM electrolysis cell as there are no temperature sensors inside the PEM electrolysis cell and the cell is assumed to have a uniform temperature throughout which is taken equal to the temperature of the water exiting the anode side. This also makes the proposed model computationally efficient and is sufficient for high-level system analysis by neglecting the spatial temperature gradients and local thermal phenomena. Of course, this assumption also has its limitations when significant localised internal heat generation occurs, or if the cell has very large dimensions or low thermal conductivity, making it unlikely for heat to distribute uniformly, however for the current study, this assumption is justified.

The thermal model is coupled with the fluidic model using multiport $R_c$ elements to take into account the enthalpy flows because of the movement of water and produced gases.The equation for the evolution of the temperature of the cell is calculated from the energy conservation equation at the zero junction and is written as [6]

$$T_{cell} = \frac{1}{C^{th}_{cell}}\int\left(\dot{H}^{in}_{cat} + \dot{H}^{in}_{ano} + \dot{Q}_H + \dot{Q}_S + \dot{Q}_{irr} - \dot{H}^{out}_{ano} - \dot{H}^{out}_{cat} - \dot{Q}_{atm}\right)\mathrm{d}t \tag{7}$$

The previous publications by the authors can be referred to undertsand the process of generation of these equations [6, 8]. However, for the presented work the governing equations for the model are generated automatically in the 20-sim software through the exploitation of the causal properties of the bond graph [19]. These generated equations for the model have been included in the appendix.

A sensitivity study has been performed using the Sensitivity Analysis option of the Time Domain Toolbox of 20-Sim software[15]. This built-in feature allows the user to analyse the effect of the variation in the parameters on the output. In presented work, the effect of the variation of the various parameters on the power loss trackers has been analysed. The dependency of the power loss estimation on these parameters is analysed through the sensitivity value for each parameter and is defined as the percent change in the power loss to the change in the parameter. The variation of $\pm 10\%$ in the parameters has been considered for this analysis. For the sensitivity study, the Integral of Absolute Value (approximated through Euler's method) metric has been chosen as it provides a robust, quantitative measure of the overall power loss deviation due to a parameter change. Six parameters have been considered for the sensitivity study, namely, thermal resistance of the cell ($R_{cell}th$), Current exchange density of anode side ($I_{0,a}$), current exchange density of cathode side ($I_{0,c}$), hydration of the membrane ($\alpha_{mem}$), thickness of the membrane ($d_{mem}$), and ohmic resistance of the cell components other than membrane ($R_{oth}$). Tables 3 and 4 show the sensitivity analysis of the power loss tracker for the electrothermal submodel and the thermal submodel, respectively. From table 3, it can be seen that the power loss tracker for electrothermal submodel is highly sensitive to the current exchange density on the cathode side and least sensitive to the current exchange density on the anode side. This power loss tracker is also partially sensitive to the thermal resistance of the cell. Therefore, the effect of thermal degradation will also contribute to power loss in electrothermal phenomena. From table 4, it can be concluded that the power loss tracker of the thermal model of the PEM electrolysis cell is highly sensitive to thermal resistance and least sensitive to the ohmic resistance of the cell. A change in the hydration level of the membrane will also contribute partially towards the power loss in the thermal domain.

Table 3. Sensitivity analysis for power loss tracker in electrothermal submodel

| **X = Parameter** | **Nominal Value x** | **dx(%)** | dy | **dy(%)** | **dy/dx Sensitivity** (%) |
|---|---|---|---|---|---|
| $R_{cell}^{th}$ | 0.5 | 1 | -2.92E-05 | -0.1317 | -13.176 |
| $I_{0,a}$ | 7.43E-08 | 1 | -9.372E-12 | -4.23E-08 | -4.230E-06 |
| $I_{0,c}$ | 0.005754 | 1 | 0.0002639 | 1.19135 | 119.135 |
| $\alpha_{mem}$ | 15 | 1 | 2.103E-06 | 0.009492 | 0.949 |
| $d_{mem}$ | 0.0046 | 1 | -2.881E-06 | -0.013005 | -1.300 |
| $R_{oth}$ | 0.05 | 1 | -3.514E-11 | -1.5859E-07 | -1.585E-05 |

Table 4. Sensitivity analysis for power loss tracker in thermal submodel

| **X = Parameter** | **Nominal Value x** | **dx(%)** | dy | **dy(%)** | **dy/dx Sensitivity** (%) |
|---|---|---|---|---|---|
| $R_{cell}^{th}$ | 0.5 | 1 | 833.848 | 1.1066 | 110.66 |
| $I_{0,a}$ | 7.43E-08 | 1 | -9.1379E-12 | -1.1441E-08 | –1.1441E-06 |
| $I_{0,c}$ | 0.005754 | 1 | 0.0002639 | 3.2976E-07 | 3.2976E-05 |
| $\alpha_{mem}$ | 15 | 1 | 3.6215E-06 | 4.5341E-09 | 4.5341E-07 |
| $d_{mem}$ | 0.0046 | 1 | -4.595E-06 | -5.753E-09 | -5.753E-07 |
| $R_{oth}$ | 0.05 | 1 | -3.513E-11 | -4.398E-14 | -4.398E-12 |

The proposed methodology has been implemented for the hybrid multi-source platform available at the University of Lille, shown in Figure 9 For the

Figure 9. Hybrid multi-source platform with PEM electrolyser at the University of Lille.

presented study, the application is focused on the key component of the PEM electrolyser, i.e. PEM electrolysis cell. Based on the availability of the measurement sensors in the physical system, the power loss trackers can be introduced to the presented bond graph model in Figure 8. The current sensor measurement is introduced to the bond graph model for the power loss tracking through PLTFS, as the current corresponds to the flow variable. Similarly, the temperature measurement and the anode and cathode side pressure measurements are introduced through PLTEs to the bond graph as they are effort variables. In the absence of the actual measurements, the measurements can be estimated from the performance bond graph model (integral causality) as shown in the figure 10. The performance model can also act as the digital twin of the PEM electrolysis cell, allowing the induction of the faults in the model itself, which is impossible to induce or emulate in the real process due to practicality issues and safety concerns. The performance model developed and demonstrated by the

authors for a single cell PEM electrolyser in [6] has been used for the simulations showing the proposed approach, presented in the following section.

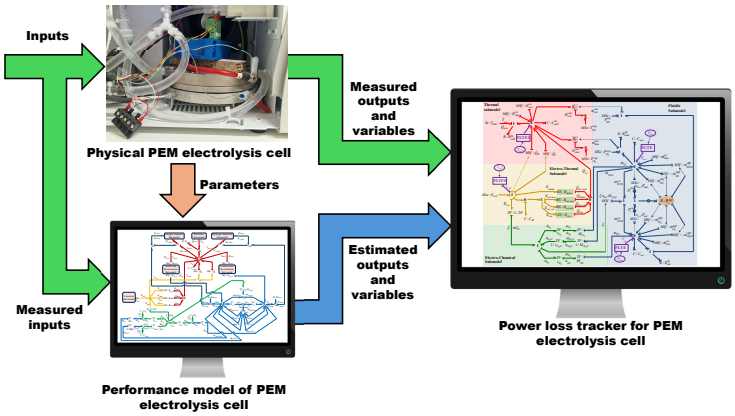


Figure 10. Implementation of the proposed approach for power loss tracking.

## 4. Simulations and Discussion

To demonstrate the effectiveness of the proposed methodology, the PEM electrolysis cell is considered to be operated at a constant voltage of 4.5V for 400 hours. The degradation is introduced directly into the performance model by changing the parameters. For this, two cases have been presented. In the first case, the degradation of the MEA has been considered to start appearing at the 50th hour of the simulation, as shown in Figure 11(a). This degradation is assumed to evolve gradually and linearly over time because of the ageing of the electrolyser cell, and it directly affects the ohmic resistance of the cell [27].It has been reported by the researchers that the ohmic resistance increases approximately linearly during the decay phase due to membrane component degradation [28, 29]. This is evident that with an increase in the ohmic resistance, the ohmic power loss increases. The same can be seen in figure 11(b), which represents the ohmic power loss due to the MEA degradation (the negative value of the power represents power loss). This power loss is directly estimated by the PLTFS placed at the 1 junction of the electro-thermal submodel. The increase in the ohmic resistance directly affects hydrogen production. With the increase in ohmic resistance, as the current decreases, the hydrogen production decreases as seen in figure 11(c). The evolution of the temperature of the cell is shown in Figure 11(d). With the increase in ohmic resistance at constant voltage, the temperature of the cell decreases due to the decrease in current.

In the second case, the thermal resistance of the cell is considered to be increasing with time. This can happen for many reasons, such as failure or degradation of the ventilation system or the heat exchange system. Under aggressive testing protocols (e.g. temperature or load cycling), interface and ma-

terial degradation accelerate rapidly, yielding an exponential growth in thermal resistance [30]. Thus, the thermal resistance of the cell is assumed to increase exponentially as shown in Figure 12(a). This increases the temperature of the cell as its heat dissipation capacity reduces, as shown in Figure 12(d). It is worth mentioning that the power loss in the case of the thermal domain is not the product of the measured effort and estimated flow, but is directly equal to the flow because the flow in this case is the heat flow rate and is equivalent to thermal power.

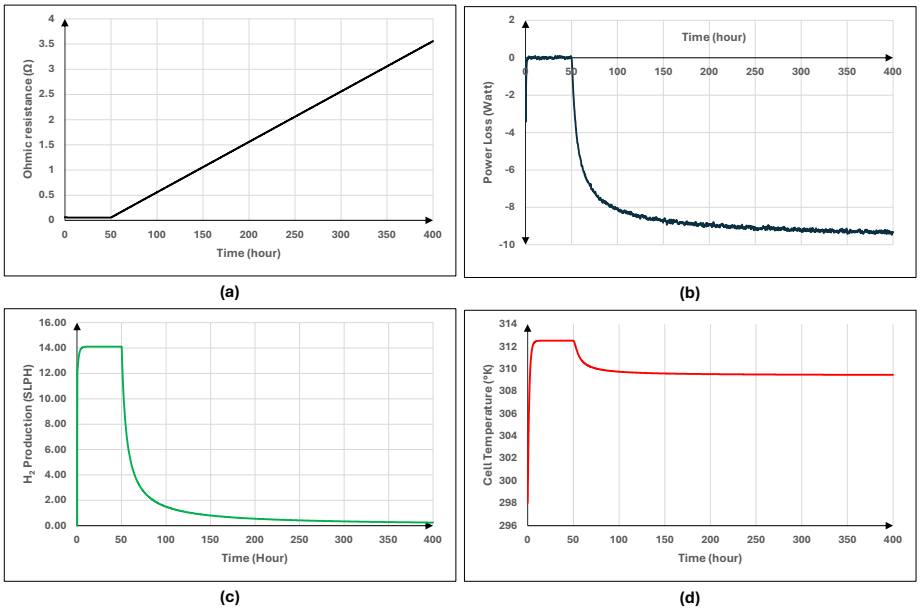


Figure 11. Simulation results for case 1: (a)Evolution of ohmic resistance, (b) Power loss estimation, (c) Hydrogen production and (d) Cell temperature evolution;

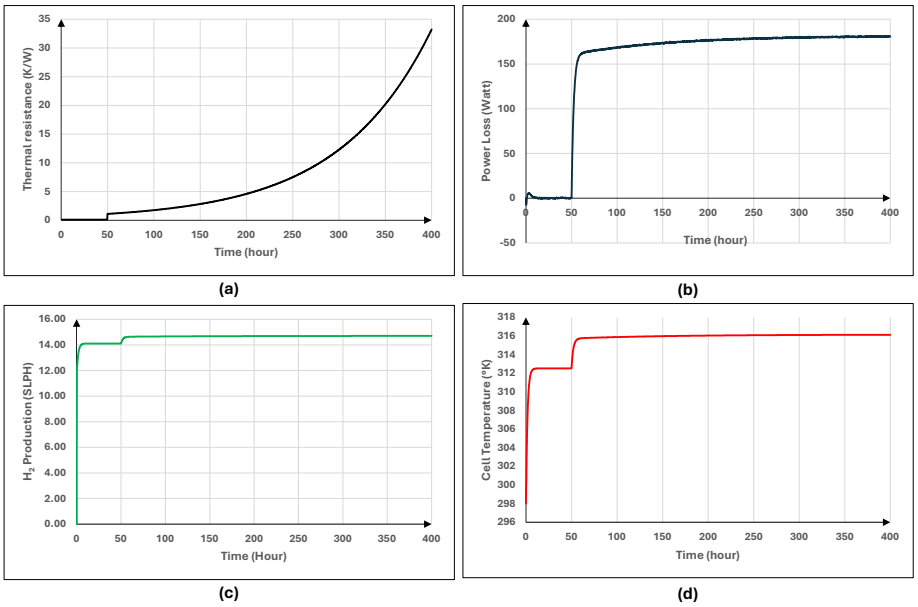


Figure 12. Simulation results for case 2: (a)Evolution of ohmic resistance, (b) Power loss estimation, (c) Hydrogen production and (d) Cell temperature evolution.

In case of the increase in thermal resistance, the power loss is shown in Figure 12(b), which is tracked by the PLTES placed at the zero junction of the thermal model. It can be seen that the value of the power loss is positive. This means that instead of power loss, the power gain has occurred, which is justified as with the increase in thermal resistance, the heat flow towards the surroundings has decreased. Figure 12(c) shows the hydrogen production for this case. The hydrogen production increases with an increase in thermal resistance as with an increase in temperature, the energy required to dissociate the water molecules also decreases.

## 5. Conclusion

Coupled Bond Graph-based power loss tracking has been presented for the PEM electrolysis cell. Two generalised power loss trackers, PLTES and PLTFS, have been introduced that can be modelled as capsules for power loss tracking using derivative bond graph models, with the application presented for the PEM electrolysis cell. A sensitivity analysis of the power trackers compared to the model parameters has also been presented. The simulation for power loss tracking in a laboratory-size single PEM electrolyser cell has been presented, where the effect of degradation can be seen on hydrogen production. The power loss in the case of an increase in ohmic resistance and power gain in the case of an increase in thermal resistance were successfully tracked. This approach

provides a valuable tool for assessing the performance of the PEM electrolysis cell. Due to generic nature of the modelling and generalization of the power loss trackers for Bond Graph, the proposed methodology can be used for PEM electrolysis stacks of laboratory and industrial size. In future work, the proposed approach can also be applied to the balance of plant of the electrolyser such as hydrogen and oxygen separators and recirculation circuits to analyse the long-term performance of the complete electrolysis system. This approach also lays the foundation for using power loss tracking for the estimation of the remaining useful life of the electrolyser by estimating the power losses over time.

## Declaration of competing interest

All of the authors declare that they have no known conflicts of interest.

## Funding

This work was supported by the European Union's Horizon Europe research and innovation programme and the Clean Hydrogen Partnership under grant agreement No 101137802 (ELECTROLIFE) and the PHC Tassili project (code: 51327SE) through a collaboration between the University of Lille, France, and the University of Setif 1, Algeria. The authors appreciate the financial support provided by these programs, which made this research possible.

## References

[1] Y. Guo, G. Li, J. Zhou, Y. Liu, Comparison between hydrogen production by alkaline water electrolysis and hydrogen production by pem electrolysis, in: IOP Conference Series: Earth and Environmental Science, Vol. 371, IOP Publishing, 2019, p. 042022.

[2] E. Nguyen, P. Olivier, M.-C. Pera, E. Pahon, R. Roche, Impacts of intermittency on low-temperature electrolysis technologies: A comprehensive review, International Journal of Hydrogen Energy 70 (2024) 474–492.

[3] J. Koponen, A. Kosonen, V. Ruuskanen, K. Huoman, M. Niemelä, J. Ahola, Control and energy efficiency of pem water electrolyzers in renewable energy systems, International journal of hydrogen energy 42 (50) (2017) 29648–29660.

[4] S. Sood, Multiphysics modelling for online diagnosis and efficiency tracking: application to green h2 production, Ph.D. thesis, Université de Lille (2021).

[5] P. Olivier, C. Bourasseau, B. Bouamama, Dynamic and multiphysic pem electrolysis system modelling: A bond graph approach, International Journal of Hydrogen Energy 42 (22) (2017) 14872–14904.

[6] S. Sood, O. Prakash, M. Boukerdja, J.-Y. Dieulot, B. Ould-Bouamama, M. Bressel, A.-L. Gehin, Generic dynamical model of pem electrolyser under intermittent sources, Energies 13 (24) (2020) 6556.

[7] S. Sood, O. Prakash, M. Boukerdja, B. Ould-Bouamama, J.-Y. Dieulot, M. Bressel, A.-L. Gehin, Model-based diagnosis of proton exchange membrane water electrolysis cell: Bond graph based approach, in: 2021 European Control Conference (ECC), IEEE, 2021, pp. 2139–2144.

[8] S. Sood, O. Prakash, J.-Y. Dieulot, M. Boukerdja, B. Ould-Bouamama, M. Bressel, Robust diagnosis of pem electrolysers using lft bond graph, International Journal of Hydrogen Energy 47 (80) (2022) 33938–33954.

[9] O. Prakash, S. Sood, M. Boukerdja, B. Ould-Bouamama, J.-Y. Dieulot, A.-L. Gehin, M. Bressel, A model-based prognosis approach to proton exchange membrane water electrolysis system, in: 2021 European control conference (ECC), IEEE, 2021, pp. 2133–2138.

[10] G. Correa, P. Marocco, P. Muñoz, T. Falagüerra, D. Ferrero, M. Santarelli, Pressurized pem water electrolysis: Dynamic modelling focusing on the cathode side, International Journal of Hydrogen Energy 47 (7) (2022) 4315–4327.

[11] D. Monopoli, C. Semeraro, M. A. Abdelkareem, A. H. Alami, A. G. Olabi, M. Dassisti, How to build a digital twin for operating pem-electrolyser system–a reference approach, Annual Reviews in Control 57 (2024) 100943.

[12] I. Zerrougui, Z. Li, D. Hissel, Physics-informed neural network for modeling and predicting temperature fluctuations in proton exchange membrane electrolysis, Energy and AI (2025) 100474.

[13] Z. Zhou, K. Ye, H. Zhang, M. Hu, F. Jiang, Y. Wang, S. Sui, A digital twin model of hydrogen production system by proton exchange membrane electrolysis, in: 2024 5th International Conference on Artificial Intelligence and Electromechanical Automation (AIEA), IEEE, 2024, pp. 40–45.

[14] K. Luo, P. Li, Y. Yan, C. Ding, Z. Liu, S. Huang, Z. Duan, L. Cai, Dynamic performance prediction of pem electrolyzers combining an electrochemical neural network model and a lumped thermal capacitance model, International Journal of Green Energy (2025) 1–18.

[15] J. F. Broenink, 20-sim software for hierarchical bond-graph/block-diagram models, Simulation Practice and Theory 7 (5-6) (1999) 481–492.

[16] J. U. Thoma, B. O. Bouamama, Modelling and simulation in thermal and chemical engineering: A bond graph approach, Springer Science & Business Media, 2000.

[17] J. U. Thoma, Introduction to bond graphs and their applications, Elsevier, 2016.

[18] F. Couenne, C. Jallut, B. Maschke, P. Breedveld, M. Tayakout, Bond graph modelling for chemical reactors, Mathematical and Computer Modelling of Dynamical Systems 12 (2-3) (2006) 159–174.

[19] W. Borutzky, Bond graph modelling of engineering systems, Vol. 103, Springer, 2011.

[20] J. T. Machado, V. M. Cunha, An introduction to bond graph modeling with applications, Chapman and Hall/CRC, 2021.

[21] F. Couenne, C. Jallut, B. Maschke, M. Tayakout, P. Breedveld, Bond graph for dynamic modelling in chemical engineering, Chemical Engineering and Processing: Process Intensification 47 (11) (2008) 1994–2003.

[22] B. Ould-Bouamana, J.-P. Cassar, Integrated bond graph modelling in process engineering linked with economic systems, in: In Proceedings of the 14th European Simulation Multiconference on Simulation and Modelling: Enablers for a Better Quality of Life, 2000, pp. 340–347.
URL https://dl.acm.org/doi/abs/10.5555/647917.739676

[23] W. Borutzky, Bond graph modelling and simulation of multidisciplinary systems–an introduction, Simulation Modelling Practice and Theory 17 (1) (2009) 3–21.

[24] K. Medjaher, A. K. Samantaray, B. O. Bouamama, Bond graph model of a vertical u-tube steam condenser coupled with a heat exchanger, Simulation Modelling Practice and Theory 17 (1) (2009) 228–239.

[25] C. Kleijn, M. Groothuis, H. Differ, 20-sim 4.2 Reference Manual, Getting Started with 20-sim, 2009.

[26] J.-H. Kim, C.-Y. Oh, K.-R. Kim, J.-P. Lee, T.-J. Kim, Electrical double layer mechanism analysis of pem water electrolysis for frequency limitation of pulsed currents, Energies 14 (22) (2021) 7822.

[27] A. S. Gago, J. Bürkle, P. Lettenmeier, T. Morawietz, M. Handl, R. Hiesgen, F. Burggraf, P. A. V. Beltran, K. A. Friedrich, Degradation of proton exchange membrane (pem) electrolysis: The influence of current density, ECS Transactions 86 (13) (2018) 695.

[28] C. Rakousky, U. Reimer, K. Wippermann, M. Carmo, W. Lueke, D. Stolten, An analysis of degradation phenomena in polymer electrolyte membrane water electrolysis, Journal of Power Sources 326 (2016) 120–128.

[29] B. Kimmel, T. Morawietz, I. Biswas, N. Sata, P. Gazdzicki, A. S. Gago, K. A. Friedrich, Investigation of the degradation phenomena of a proton exchange membrane electrolyzer stack by successive replacement of aged components in single cells, ACS Sustainable Chemistry & Engineering 13 (11) (2025) 4330–4340.

[30] E. Kuhnert, K. Mayer, M. Heidinger, C. Rienessel, V. Hacker, M. Bodner, Impact of intermittent operation on photovoltaic-pem electrolyzer systems: a degradation study based on accelerated stress testing, International Journal of Hydrogen Energy 55 (2024) 683–695.